Physica Medica 62 (2019) 83–94

Contents lists available at ScienceDirect

Physica Medica

journal homepage: www.elsevier.com/locate/ejmp

Original paper

# Impact of plan parameters and modulation indices on patient-specific QA results for standard and stereotactic VMAT

Minsoo Chun[a,b,c], Hyun Joon An[a,b], Ohyun Kwon[b], Do Hoon Oh[d], Jong Min Park[a,b,c,e], Jung-in Kim[a,b,c,*]

[a] Department of Radiation Oncology, Seoul National University Hospital, Seoul, Republic of Korea
[b] Biomedical Research Institute, Seoul National University Hospital, Seoul, Republic of Korea
[c] Institute of Radiation Medicine, Seoul National University Medical Research Center, Seoul, Republic of Korea
[d] Department of Radiation Oncology, Chung-Ang University Hospital, Seoul, Republic of Korea
[e] Center for Convergence Research on Robotics, Advanced Institutes of Convergence Technology, Suwon, Republic of Korea

ARTICLE INFO

*Keywords:*
VMAT/SABR
Patient-specific QA
Plan parameters
Modulation indices

ABSTRACT

*Purpose:* To demonstrate the impact of modulation indices and plan parameters on the gamma passing rates (GPR) of patient-specific quality assurance of standard and stereotactic volumetric modulated arc therapy (VMAT) plans.

*Methods:* A total of 758 patients' QA plans were utilized, including standard VMAT plans with Trilogy ($n$ = 87, group A) and TreuBeam STx ($n$ = 332, group B), and 339 stereotactic VMAT plans with TrueBeam STx (group C). Modulation indices were obtained considering the speed and acceleration of the multileaf collimator (MLC) ($MI_s$, $MI_a$), and MLC, gantry speed, and dose rate changes ($MI_t$). The mean aperture size (MA), monitor unit (MU), and amount of jaw tracking (%JT) were acquired. Gamma analysis was performed with 2 mm/2% and 1 mm/2% for the standard and stereotactic VMAT plans, respectively. Statistical analyses were performed to investigate the correlation between modulation index/plan parameters and GPR.

*Results:* Spearman's rank correlation to GPRs with $MI_s$, $MI_a$, and $MI_t$, were −0.44, −0.45, and −0.46 for group A; −0.39, −0.37, and −0.38 for group B; and −0.04, −0.11, and −0.10 for group C, respectively. While MU and MA showed significant correlations in all groups, %JT showed a significant correlation only with stereotactic VMAT plans. The most influential parameter combinations were MU-MA ($r_s$ = 0.50), $MI_s$-%JT ($r_s$ = 0.43), and MU-%JT ($r_s$ = 0.38) for groups A, B, and C, respectively.

*Conclusions:* MLC modulation mostly affected the GPR in the delivery of standard VMAT plans, while MU and %JT showed more importance in stereotactic VMAT plans.

## 1. Introduction

Volumetric modulated arc therapy (VMAT) makes it possible to deliver a prescription dose to a target volume while minimizing any complications involving normal tissue by simultaneously modulating the multileaf collimator (MLC), dose rate, and gantry speed [1–4]. Furthermore, stereotactic ablative radiotherapy (SABR) administers a higher dose than conventional fractionated radiation therapy with a single or up to five fractions, which necessitates higher accuracy and precision of beam delivery [5–10]. The administration of these highly complex treatments should be dosimetrically verified in advance, and this is typically performed through gamma analysis by comparing the calculated and measured doses with a two-dimensional (2D) array detector or portal dose image prediction (PDIP) [11–18].

Although three-dimensional (3D) patient-specific QA became available with 3D gels and PRESAGE dosimeters, these approaches are not yet widely available owing to their instability caused by storage circumstances, manufacturing processes, and limitations in reuse [19–22]. In addition to 3D dosimeters, 2D measurement-based pseudo-3D reconstruction also enabled 3D gamma analysis; however, a large discrepancy between EPID-based 3D reconstruction and 3D PAGAT gel dosimetry was reported. In turn, a perfect 3D-based GPR evaluation has not been established yet [23].

Although numerous parameters can influence the precision and accuracy of beam delivery in VMAT, the results of many studies indicated that the degree of modulation was the primary parameter that

* Corresponding author at: Department of Radiation Oncology, Seoul National University Hospital, 101 Daehak-ro, Jongno-gu, Seoul 03080, Republic of Korea.
*E-mail address:* madangin@gmail.com (J.-i. Kim).

https://doi.org/10.1016/j.ejmp.2019.05.005
Received 5 November 2018; Received in revised form 3 May 2019; Accepted 4 May 2019
Available online 10 May 2019

introduced uncertainties in the VMAT delivery process and thereby had the most significant impact on gamma passing rates (GPR) [24]. To quantify the beam intensity modulation of VMAT plans, Park et al. devised modulation indices that represent the speed and acceleration of the MLC, gantry speed change, and the dose rate change ($MI_t$). A significant correlation to local GPRs with 2%/2 mm criteria was found in prostate and head-and-neck VMAT plans [24].

Masi et al. established the concept of a modulation complexity score by considering the leaf sequence variability, positional variations, and monitor unit (LTMCS), and a significant correlation was found between the LTMCS and GPR [25]. A similar study with helical tomotherapy pretreatment QA reported a strong correlation between GPR and various parameters such as the gamma method (global or local), irradiated length, pitch, maximum dose to the diodes, and dose per fraction, while the modulation factor showed no dependence on GPR. This study is noteworthy in that a large amount of data (384 patient plans) was used to demonstrate a direct relationship between the actual delivery parameters and GPR [26]. In addition to the modulation indices, the use of jaw tracking by arranging the field aperture closest to the planning target volume (PTV) for each control point is known to potentially minimize the interleaf leakage, thereby allowing for a dose reduction in organs at risk (OARs) [27–29]. Furthermore, it was reported that the maximum field size might not be a factor influencing the dosimetric uncertainties in intensity modulated radiation therapy (IMRT) for symmetric fields [30].

Although several studies validated the dosimetric accuracy in terms of the modulation indices and plan parameters, more rigorous investigations are still needed, comprehensively concerning the types of MLCs and detectors, treatment techniques, jaw tracking availability, aperture size, and monitor units (MUs), as well as modulation indices with a large amount of data. In this study, modulation indices suggested by Park *et al.* and several plan parameters such as the mean aperture size, total MU, and percentage of jaw tracking are employed. A relatively large amount and various kinds of data are included concerning the treatment techniques (standard vs. stereotactic VMAT) and the types of detector (diode array vs. portal dosimetry). Furthermore, the most predictable parameter combinations during standard and stereotactic VMAT delivery were estimated by using multi parameter regression approaches.

## 2. Materials and methods

### 2.1. Patient selection and treatment planning

A total of 758 patients who underwent VMAT treatment at our institute from April 2014 to April 2017 were retrospectively selected for this study. Treatment sites included the head and neck (HN), brain, craniospinal irradiation (CSI), spine, lung, liver, abdomen, and prostate. The corresponding prescription doses and fraction of the patients were varied depending on the treatment sites, underlying disease (or metastasis), and the clinical protocols from the physician. In the cases of patients with tumors located in the spine, lung, liver, and abdomen, stereotactic ablative radiotherapy (SABR) was prescribed.

VMAT plans were generated by the Eclipse™ (Varian Medical Systems, Palo Alto, CA) treatment planning system (TPS). Two VMAT machines available in our institute were used: Trilogy™ (TRG, Varian Medical Systems, Palo Alto, CA, USA) equipped with a 120 Millennium MLC, and TrueBeam STx™ (TBX, Varian Medical Systems, Palo Alto, CA, USA) equipped with a high-definition 120 MLC (HD120 MLC). Because flattening-filter-free (FFF) modes for 6 MV and 10 MV were available in TBX, all stereotactic plans were generated with TBX. Based on the location of the tumors and the OARs, the gantry angles and the couch rotation angles were determined.

Two partial-arc plans were used for lung and liver patients, while two full-arc plans were utilized for the others. Each VMAT plan was optimized by using the progressive resolution optimizer 3 (PRO3, Ver. 10.0.28, Varian Medical System, Palo Alto, CA, USA), and an analytical anisotropic algorithm (AAA, Ver. 10.0.28, Varian Medical System, Palo Alto, CA, USA) was used for dose calculation with 2-mm and 1-mm calculation grid sizes for standard and SABR plans, respectively. Patients were categorized into three groups according to the machine and treatment prescription: group A was with the standard VMAT in TRG, group B was with the standard VMAT in TBX, and group C was with the stereotactic VMAT in TBX.

### 2.2. Verification plan and gamma analysis

The treatment plans, with unaltered parameters, were recalculated by replacing the reference images with those of the detectors for QA purposes. Two kinds of detectors were used: the 2D array diode detector MapCHECK2™ (Sun Nuclear Corporation, Melbourne, FL, USA) inserted into MapPHAN™ (Sun Nuclear Corporation, Melbourne, FL, USA), and the aS1000 detector-based portal dose image prediction (PDIP, Ver. 10.0.28, Varian Medical Systems, Palo Alto, CA, USA). In case of MapCHECK2, the detector was placed horizontally where the isocenter of the treatment plans corresponded to the center of the detector. The dose distribution for the verification plan with MapCHECK2™ was calculated using the AAA algorithm, and the PDIP algorithm was used for those delivered into an electronic portal imaging device (EPID). The calculation grid size for both QA plans was 1 mm. Since the EPID application with an aS1000 detector does not allow for portal dosimetry in flattening-filter-free beam mode [31], MapCHECK2™ with MapPHAN™ was assigned to groups A and C, and PDIP was used for group B.

SNC patient™ software (ver. 6.6.0, Sun Nuclear Corporation, Melbourne, FL, USA) was used to perform 2D gamma analysis with MapCHECK2™, and the gamma criteria were 2 mm/2% for the standard VMAT plans (group A and B) and 1 mm/2% for the stereotactic VMAT plans (group C) [11]. A portal dosimetry module embedded in Eclipse™ TPS was used to perform 2D gamma analysis with PDIP, where the gamma criteria were 2 mm/2%. The threshold value was 10%, *i.e.*, the points with calculated doses equal to or less than 10% of the maximum doses were ignored when calculating the GPR. The global gamma analysis was used, *i.e.*, the percent dose differences of each point were calculated relative to the maximum dose.

### 2.3. Plan parameters and modulation indices

With DICOM RT Plan objects exported from Eclipse TPS, plan parameters such as MU and mean aperture size (MA, $cm^2$) for all control points were obtained. In the case of groups B and C, the percentage of jaw tracking (%JT) was also calculated by counting the number of control points with changes in the collimator size to closely fit to the apertures, divided by the total number of control points.

VMAT is known to deliver photon beams by modulating the gantry rotation speed, dose rate, and MLC speed. In this regard, the modulation indices presented by Park et al. were calculated considering the speed of MLC ($MI_s$), acceleration of the MLC ($MI_a$), both MLC speed and acceleration, gantry rotation variation, and dose rate variation ($MI_t$) [24,32]. The numerical derivations for $MI_s$, $MI_a$, and $MI_t$ are summarized in Appendix A.

### 2.4. Statistical analysis

All statistical analyses were performed by employing SPSS Statistics for Windows (Version 22.0. IBM Corporation, Armonk, NY). The mean and standard deviations of the plan parameters, modulation indices, and GPR were calculated for each group. Spearman's rank correlation coefficients ($r_s$) of the plan parameters and modulation indices of the GPR were calculated for each group, and *p*-values were obtained under the two-tail paired condition at a 95% confidence level. For each group, a principal component analysis (PCA) was performed to select the most influential modulation indices and plan parameters without

**Table 1**
Mean ± standard deviation of plan parameters, modulation indices, and GPR according to treatment sites.

| Group | | Treatment sites | | | | | | | |
|---|---|---|---|---|---|---|---|---|---|
| | | HN[a] | Brain | CSI[b] | Spines | Lung | Liver | Abdomen | Prostate |
| A | No. | | | 9 | 21 | 24 | | 33 | |
| | MU[c] | | | 266.64 ± 36.55 | 694.01 ± 345.15 | 548.05 ± 136.46 | | 442.92 ± 149.54 | |
| | MA[d] ($cm^2$) | | | 98.20 ± 36.93 | 53.85 ± 34.61 | 45.12 ± 16.69 | | 62.03 ± 38.81 | |
| | $MI_s$[e] | | | 17.45 ± 2.77 | 26.31 ± 12.44 | 26.33 ± 7.63 | | 26.95 ± 11.39 | |
| | $MI_a$[f] | | | 25.13 ± 2.77 | 39.06 ± 20.24 | 40.74 ± 13.26 | | 39.37 ± 16.99 | |
| | $MI_t$[g] | | | 24.79 ± 5.94 | 38.71 ± 20.96 | 41.20 ± 13.30 | | 39.61 ± 17.20 | |
| | GPR[h] (%) | | | 96.66 ± 3.80 | 98.38 ± 3.80 | 97.10 ± 1.42 | | 98.18 ± 2.00 | |
| B | No. | 29 | 23 | | 47 | 31 | 11 | 92 | 99 |
| | MU | 459.41 ± 123.66 | 476.86 ± 155.45 | | 967.05 ± 435.69 | 580.74 ± 195.31 | 740.17 ± 314.20 | 410.68 ± 124.70 | 624.55 ± 133.00 |
| | %JT[i] | 30.51 ± 14.95 | 28.83 ± 8.70 | | 24.60 ± 9.20 | 38.36 ± 10.58 | 22.16 ± 9.92 | 31.33 ± 11.21 | 33.60 ± 11.87 |
| | MA ($cm^2$) | 37.06 ± 24.76 | 52.98 ± 31.66 | | 40.43 ± 22.86 | 49.93 ± 21.52 | 38.97 ± 20.12 | 36.73 ± 19.09 | 34.22 ± 23.13 |
| | $MI_s$ | 40.25 ± 16.09 | 40.03 ± 10.96 | | 33.72 ± 12.24 | 41.19 ± 14.10 | 30.67 ± 13.22 | 31.76 ± 9.47 | 32.80 ± 16.02 |
| | $MI_a$ | 57.76 ± 23.70 | 56.62 ± 14.46 | | 47.87 ± 18.44 | 60.85 ± 20.95 | 43.49 ± 19.47 | 45.18 ± 14.46 | 45.42 ± 23.55 |
| | $MI_t$ | 58.80 ± 24.32 | 57.29 ± 14.27 | | 48.34 ± 18.64 | 61.83 ± 21.17 | 43.84 ± 19.66 | 45.33 ± 14.59 | 45.74 ± 23.73 |
| | GPR (%) | 97.11 ± 2.49 | 95.95 ± 3.32 | | 97.73 ± 2.44 | 97.95 ± 2.19 | 97.00 ± 2.75 | 98.74 ± 1.53 | 98.37 ± 1.96 |
| C | No. | | | | 120 | 134 | 33 | 52 | |
| | MU | | | | 4716.80 ± 2167.51 | 3871.75 ± 692.33 | 3068.51 ± 1189.78 | 2585.36 ± 895.41 | |
| | %JT | | | | 22.53 ± 7.40 | 7.85 ± 5.49 | 19.12 ± 8.69 | 15.42 ± 8.40 | |
| | MA ($cm^2$) | | | | 18.89 ± 16.41 | 6.88 ± 3.31 | 13.86 ± 9.39 | 11.72 ± 7.86 | |
| | $MI_s$ | | | | 16.71 ± 8.38 | 10.13 ± 2.78 | 11.87 ± 6.43 | 11.78 ± 7.99 | |
| | $MI_a$ | | | | 24.56 ± 12.74 | 13.25 ± 3.86 | 17.36 ± 10.11 | 17.00 ± 11.95 | |
| | $MI_t$ | | | | 24.62 ± 12.82 | 13.31 ± 3.89 | 17.39 ± 10.12 | 17.08 ± 12.06 | |
| | GPR (%) | | | | 95.05 ± 2.51 | 96.88 ± 2.81 | 96.66 ± 2.13 | 97.01 ± 1.94 | |

[a] HN: head and neck.
[b] CSI: craniospinal irradiation.
[c] MU: monitor unit.
[d] MA: mean aperture size.
[e] $MI_s$: modulation index considering speed of multileaf collimator.
[f] $MI_a$: modulation index considering acceleration of multileaf collimator.
[g] $MI_t$: modulation index considering speed and acceleration of multileaf collimator, and gantry rotation acceleration and dose rate variation.
[h] GPR: gamma passing rate.
[i] %JT: percentage of jaw tracking.

dependencies between variables.

Multivariate linear regressions were performed by employing two candidate parameters from the PCA results, and their corresponding unstandardized coefficient was acquired [33]. To remove the impact of the parameter size and to allow for an intuitive interpretation of the prediction model, each variable was normalized and renamed as a standardized coefficient, as follows: $Z = (X - \mu_X)/\sigma_X$, where $X$, $\mu_X$, and $\sigma_X$ denote the parameter, mean, and standard deviation, respectively. The standardized coefficient ($\beta$) was then acquired by multivariate linear regression with normalized parameters.

## 3. Results

### 3.1. Plan parameters

The basic plan parameters according to each group and treatment sites are provided in Table 1. It was shown that the average and standard deviation of %JT was 31.2 ± 11.9% and 15.3 ± 9.5% for groups B and C, respectively. This shows that for stereotactic plans, the collimator possessed similar jaw openings with those of adjacent control points. The use of jaw tracking in group B was more frequent than group C, while the mean aperture size for group B was 3.1 times larger than those for group C. Although there were differences in the prescription dose according to the treatment sites and the protocols from the physician, the total MUs in group C were approximately 7.6 and 6.6 times higher than those for groups A and B, respectively.

### 3.2. Modulation indices

The mean and standard deviation of the modulation indices are summarized in Table 1. In group B, it can be seen that $MI_s$, $MI_a$, and $MI_t$ for the head and neck (HN) simultaneous integrated boost (SIB) plans were approximately 1.3 times higher than those for the prostate plans, which is in accordance with previous research [24]. Furthermore, the modulation indices of lung plans where the locations of OAR were adjacent to the target volume were higher than those of the liver, spine, abdomen, and prostate plans. In group C, $MI_s$, $MI_a$, and $MI_t$ for the spine, lung, liver, and abdomen plans showed similar levels. Because SABR is usually associated with tumor lesions less than 5 cm in maximum diameter, the extent of modulation was limited by its mathematical definition, showing about 2.7 times higher $MI_s$, $MI_a$, and $MI_t$ for group B than those for group C [34].

### 3.3. Gamma passing rates

The mean and standard deviation of the GPRs are summarized in Table 1. Since global GPRs higher than 90% with 2 mm/2% in standard VMAT QA and 1 mm/2% in stereotactic VMAT QA have been recommended as the acceptable gamma criteria [35,36], our GPR results could be regarded as acceptable for treatment as they showed 97.8 ± 2.0%, 98.0 ± 2.3%, and 96.2 ± 2.7% for group A, B, and C, respectively.

### 3.4. Correlation analysis

Spearman's rank correlation coefficients ($r_s$) and their corresponding $p$-values according to each group are provided in Table 2. In group A, statistical significances with GPR were found for all parameters, although the highest correlation was found with $MI_t$. The negative $r_s$ for $MI_s$, $MI_a$, and $MI_t$ indicates that a low GPR was induced by higher degrees of modulation, although these three indices demonstrated a similar level of $r_s$, implying that the major contribution to the GPR remained with the MLC modulation. In group B, where all parameters were kept the same as those of group A except for the use of jaw tracking and HD MLC, a significant correlation with GPR was found in MU, MA, $MI_s$, $MI_a$, and $MI_t$, but not with %JT. This indicates that jaw tracking did not significantly impact the GPR in standard VMAT, and the MLC modulation remained the most influencing factor even with the introduction of HD MLC and jaw tracking availability.

Meaningful findings were obtained for group C, which revealed that the major contributions to the GPR were with MU, %JT, and MA, but not with $MI_s$, $MI_a$, or $MI_t$. The differences in the mean aperture sizes between groups B and C induced different degrees of modulation. Although for standard VMAT the MLC modulation was the most influential factor on the GPR in agreement with the literature, significant correlations with MU and %JT were observed in stereotactic VMAT. The relationships between the GPR and the plan parameters or modulation indices in groups A, B, and C are shown in Figs. 1–3, respectively.

For all groups, the PCA results showed that $MI_s$, $MI_a$, and $MI_t$ closely correlated with each other and were mutually exclusive to other plan parameters such as MU, MA, and %JT, as shown in Fig. 4. Therefore,

**Table 2**
Overall GPR statistics and Spearman's rank correlation coefficients ($r_s$) and their corresponding $p$-values between GPR (%) and modulation index or plan parameters.

| | $r_s$[a]($p$) | | |
|---|---|---|---|
| | Group A | Group B | Group C |
| No. | 87 | 332 | 339 |
| Detector types | MapCHECK2 | PDIP[b] | MapCHECK2 |
| Gamma criteria | 2 mm/2% | 2 mm/2% | 1 mm/2% |
| Gamma passing rate | 97.8 ± 2.0% | 98.0 ± 2.3% | 96.2 ± 2.7% |
| MU[c] | −0.433 (< 0.001) | −0.116 (0.034) | −0.299 (< 0.001) |
| %JT[d] | – | −0.036 (0.513) | −0.265 (< 0.001) |
| MA[e] ($cm^2$) | −0.344 (0.002) | −0.250 (< 0.001) | −0.180 (0.001) |
| $MI_s$[f] | −0.442 (< 0.001) | −0.392 (< 0.001) | −0.044 (0.417) |
| $MI_a$[g] | −0.445 (< 0.001) | −0.374 (< 0.001) | −0.108 (0.047) |
| $MI_t$[h] | −0.459 (< 0.001) | −0.375 (< 0.001) | −0.102 (0.060) |

[a] $r_s$: Spearman's correlation coefficient.
[b] PDIP: portal dose image prediction.
[c] MU: monitor unit.
[d] %JT: percentage of jaw tracking.
[e] MA: mean aperture size.
[f] $MI_s$: modulation index considering speed of multileaf collimator.
[g] $MI_a$: modulation index considering acceleration of multileaf collimator
[h] $MI_t$: modulation index considering speed and acceleration of multileaf collimator, and gantry rotation acceleration and dose rate variation.

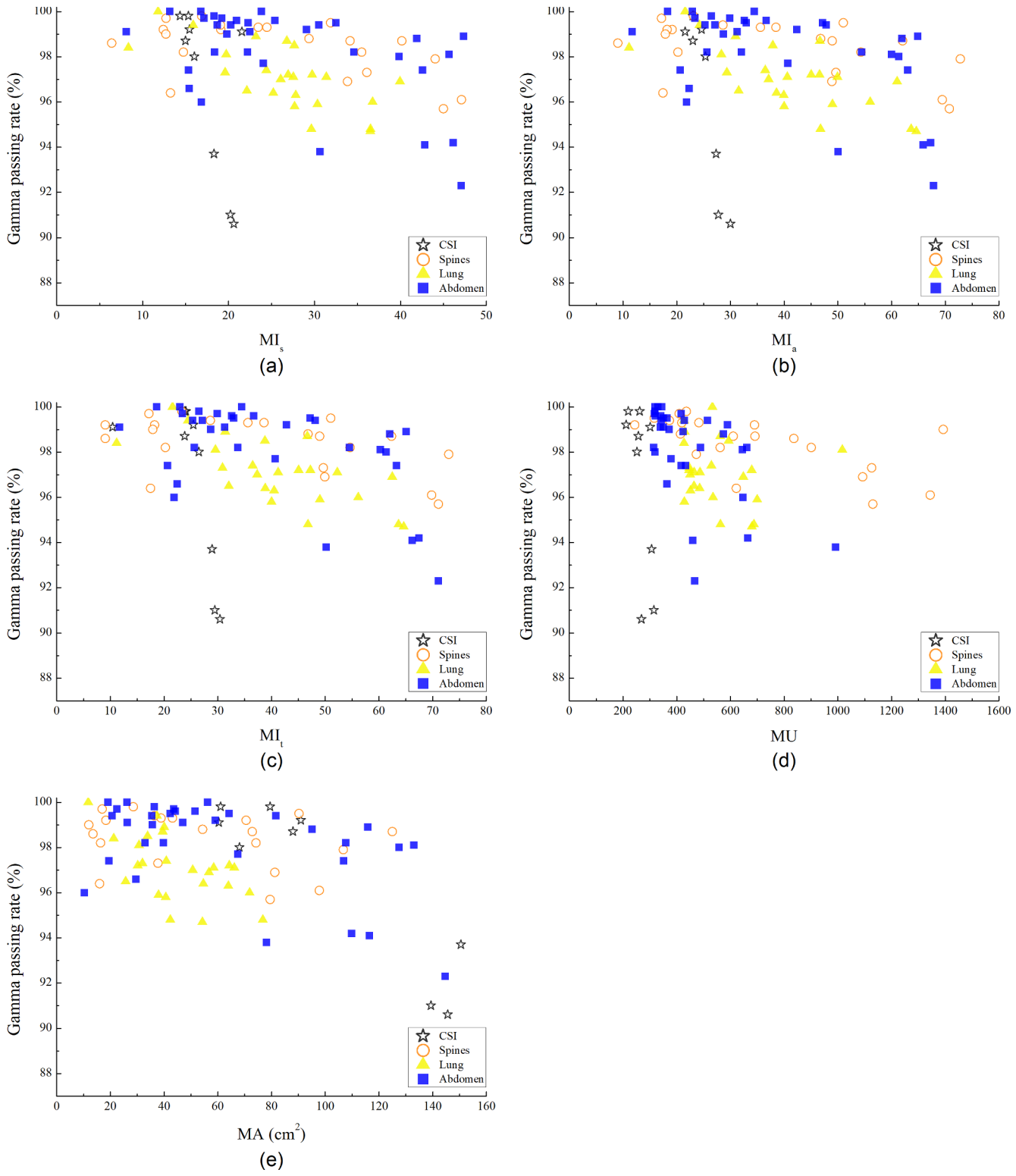


**Fig. 1.** Scatter plots between GPR and plan parameters or modulation indices for group A for (a) $MI_s$, (b) $MI_a$, (c) $MI_t$, (d) MU, and (e) MA. Legends denote treatment sites.

one representative modulation index ($MI_s$) and three plan parameters were selected as candidate parameters. A summary of a multivariate analysis is presented in Table 3. For group A, the mean aperture and total MU along with the degree of modulation similarly impacted the GPRs. In particular, the combination of MU and MA exhibited the highest $r_s$ of 0.50 and showed a statistically significant difference for $\beta$.

For group B, the combination of $MI_s$ and %JT showed statistical significance and the highest $r_s$ of 0.43 ($p < 0.001$). Except for the MU-%JT combination, all parameter combinations showed a statistical significance. For group C, the combination of MU and %JT showed the highest correlation with $r_s$ of 0.38 ($p < 0.001$), which was higher than any combination with $MI_s$. Fig. 5 presents the correlation between the best representative parameter combinations and their corresponding GPRs for each group.

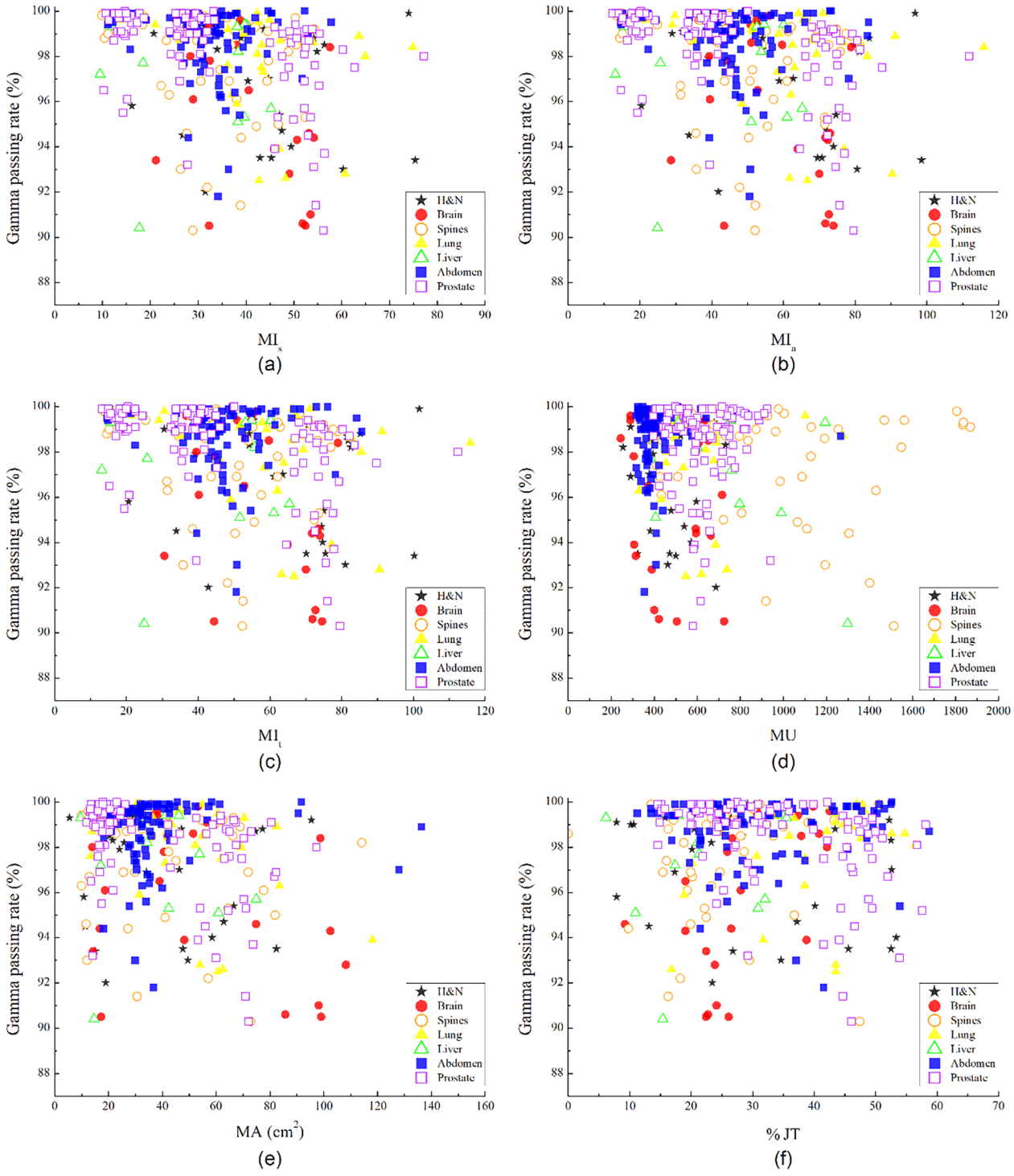


**Fig. 2.** Scatter plots between GPR and plan parameters or modulation indices for group B for (a) $MI_s$, (b) $MI_a$, (c) $MI_t$, (d) MU, and (e) MA, and (f) %JT. Legends denote treatment sites.

## 4. Discussion

It has been validated through numerous studies that the MLC modulation mostly impacted the GPRs in VMAT QA [24,25,32]. Park et al. defined comprehensive modulation indices by incorporating the speed, acceleration of the MLC, and changes in gantry speed and dose rate ($MI_s$, $MI_a$, and $MI_t$) [24]. In the validation of the modulation indices with 60 patients' VMAT plans, three indices showed a comparable correlation with GPR, which indicates that the MLC modulation could be regarded as the most predictable indicator in VMAT delivery. Masi et al. designed the leaf travel modulation complexity score to quantitatively assess the complexity of a plan by using the MLC position, and demonstrated that this metric could potentially optimize the creation and verification of a VMAT plan [25].

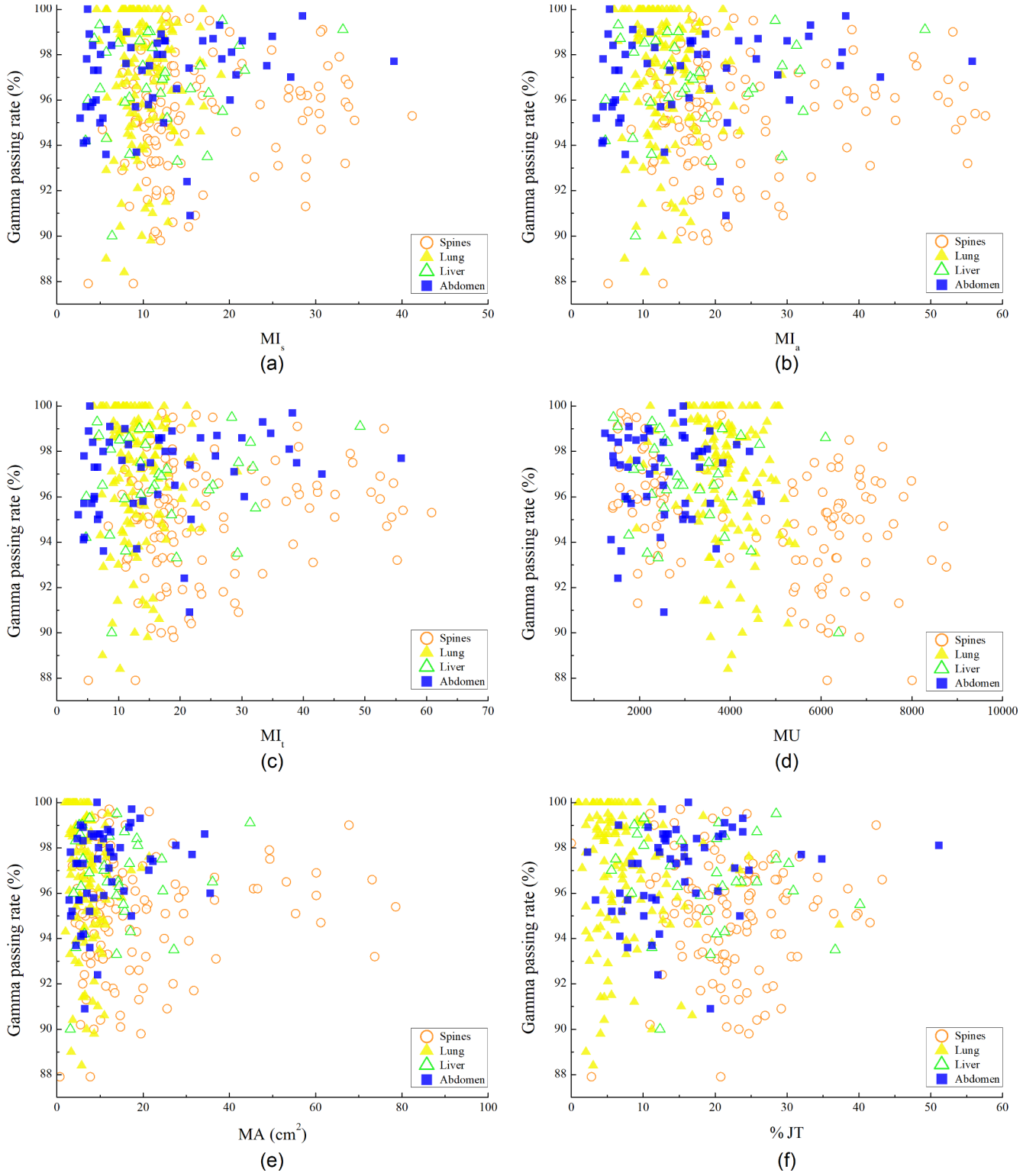


**Fig. 3.** Scatter plots between GPR and plan parameters or modulation indices for group C for (a) $MI_s$, (b) $MI_a$, (c) $MI_t$, (d) MU, and (e) MA, and (f) %JT. Legends denote treatment sites.

In another investigation, texture features based on a fluence map were retrospectively calculated, and this showed a significant correlation between the texture features and the previously devised modulation indices, which employed the MLC modulation as the first priority [37]. The correlation analysis in our study revealed a significant correlation between $MI_s$ and GPR for groups A and B, while group C did not show any significant correlation. By contrast, stronger relationships to the GPR were observed with the MU and %JT parameters in group C ($r_s = -0.30$ for MU and $-0.27$ for %JT). By employing the total MU in $MI_t$, a slight improvement in the correlation was found, although no statistical significance was observed ($p = 0.060$). The power to predict the plan deliverability tended to highlight MA, MU, and %JT instead of MLC modulation in stereotactic VMAT plans.

Du et al. demonstrated that a small plan aperture could influence

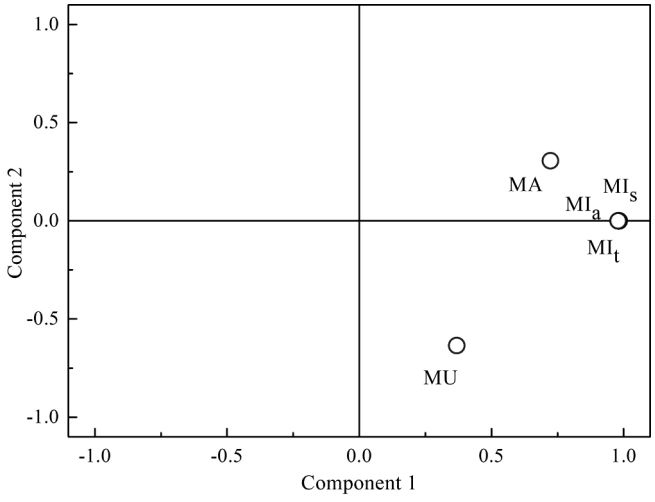


(a)

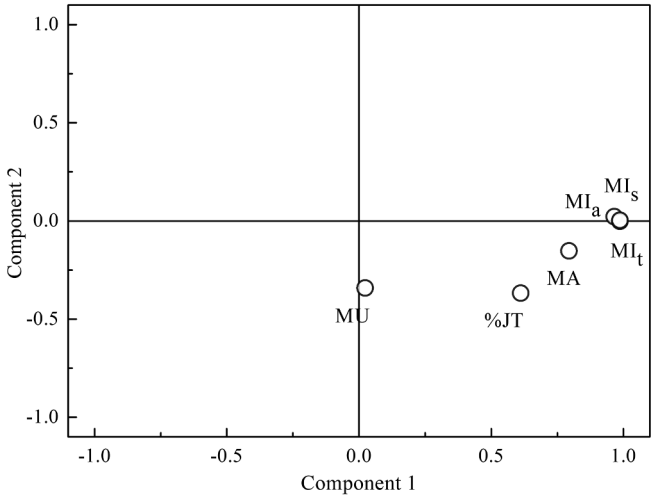


(b)

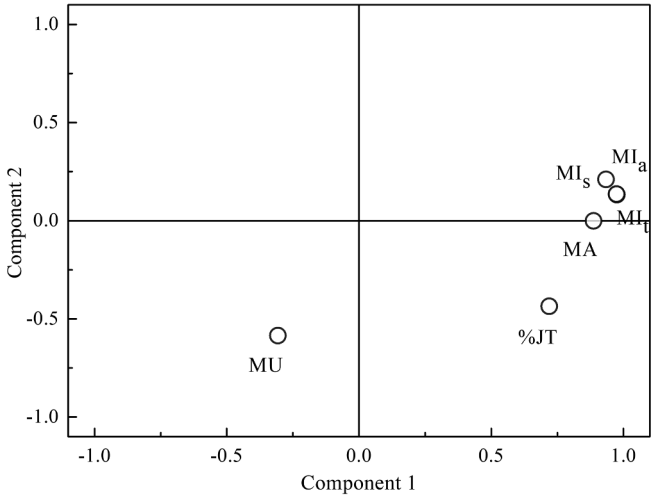


(c)

**Fig. 4.** Results of PCA analysis for each group: (a) A, (b) B, and (c) C.

**Table 3**
Multivariate analysis results showing impact of parameter combinations and their corresponding $r_s$ with GPR.

| Group | Parameter combination | | $\beta$[a] ($p$-value) | | $r_s$[b] ($p$-value) |
|---|---|---|---|---|---|
| | 1stparameter | 2ndparameter | 1stparameter | 2ndparameter | |
| A | MU[c] | $MI_s$[d] | −0.106 (0.328) | −0.321 (0.004) | 0.476 (< 0.001) |
| | MU | MA[e] | −0.247 (0.009) | −0.502 (< 0.001) | 0.500 (< 0.001) |
| | $MI_s$ | MA | −0.073 (0.560) | −0.439 (0.001) | 0.378 (< 0.001) |
| B | MU | $MI_s$ | −0.088 (0.091) | −0.318 (< 0.001) | 0.398 (< 0.001) |
| | MU | MA | −0.112 (0.033) | −0.292 (< 0.001) | 0.300 (< 0.001) |
| | MU | %JT[f] | −0.117 (0.035) | −0.038 (0.495) | 0.128 (0.019) |
| | $MI_s$ | MA | −0.234 (0.001) | −0.133 (0.060) | 0.379 (< 0.001) |
| | $MI_s$ | %JT | −0.411 (< 0.001) | 0.176 (0.003) | 0.425 (< 0.001) |
| | MA | %JT | −0.338 (< 0.001) | 0.113 (0.049) | 0.278 (< 0.001) |
| C | MU | $MI_s$ | −0.398 (< 0.001) | −0.145 (0.008) | 0.343 (< 0.001) |
| | MU | MA | −0.391 (< 0.001) | −0.170 (0.001) | 0.362 (< 0.001) |
| | MU | %JT | −0.334 (< 0.001) | −0.174 (0.001) | 0.376 (< 0.001) |
| | $MI_s$ | MA | 0.113 (0.172) | −0.150 (0.070) | 0.195 (< 0.001) |
| | $MI_s$ | %JT | 0.136 (0.028) | −0.265 (< 0.001) | 0.285 (< 0.001) |
| | MA | %JT | 0.080 (0.232) | −0.242 (< 0.001) | 0.261 (< 0.001) |

[a] $\beta$: Standardized coefficient acquired by multivariate linear regression with normalized parameters.
[b] $r_s$: Spearman's correlation coefficient.
[c] MU: monitor unit.
[d] $MI_s$: modulation index considering speed of multileaf collimator.
[e] MA: mean aperture size.
[f] %JT: percentage of jaw tracking.

the point dose discrepancy in IMRT QA [38] J. Götstedt found linear correlations with GPR for the aperture area, and converted the aperture metric measured by EPID and EBT3 film [39]. Another modulation parameter study with a helical tomotherapy machine verified that the field width influences the local GPR to 3 cGy with significant correlation [26]. The mean aperture size in our study showed significant correlations with GPRs of −0.34, −0.25, and −0.18 for groups A, B, and C, respectively. These tendencies were in accordance with those of previous studies, although the beam was delivered by binary MLC modulation with a helical fashion in the tomotherapy study. Moreover, the use of jaw tracking is known to substantially reduce the OAR dose [27,40]. In this study, we counted the control points for any jaws that were changed among all control points in each plan for groups B and C. Even with jaw tracking, %JT did not exceed 40% for all patient plans, which implies that the adjacent control points consisted of similar closest apertures.

A significant negative correlation coefficient between %JT and GPR was obtained in group C. Because the collimator moves continuously to closely fit the MLC apertures while the gantry rotates simultaneously, the majority of uncertainties can be induced not only by MLC positioning but also jaw positioning, and this tendency is more critical in smaller field apertures with a higher MU (group C). The strategies to minimize the dose calculation uncertainties for small target volumes, such as fixing the collimator at $3 \times 3\,cm^2$ when jaw tracking leads to jaw-defined field sizes smaller than $3 \times 3\,cm^2$, can be further assessed to integrate them with our study outcome [28].

Son et al. compared the 2D gamma analysis for five IMRT plans between the calculated dose and measurements with various detectors, and showed that the GPR differences between detectors are caused by the detector resolution, especially in regions with steep dose gradients [13]. Another study demonstrated that GPRs with 2%/2 mm and 3%/3 mm criteria were higher with PDIP than those with the MapCHECK2 diode array, albeit no statistical difference was found [41].

Although an average GPR in group B (standard VMAT, HD MLC with PDIP) showed the highest value in this study, and PDIP is generally known to be more sensitive to detecting errors than others owing to its superior resolution [41], we cannot conclude that the study results are in line with the literature because the GPR is obtained with different plans and gamma criteria according to each group. While several studies asserted that the diode array detector showed an angular dependency from 20% to 37% at a perpendicular beam incidence (90°), this can be reduced to about 2% at 90 ± 5°, and this can be neglected in VMAT plans because the amount of lateral beam incidence has a low weight [42–46].

To validate the overall plan accuracy, the patient-specific QA procedure has evolved from one-dimensional point dose measurement to 2D and 3D approaches. Three-dimensional approaches became available with 3D detectors such as PRESAGE dosimeters and 3D gels, as well as 2D measurement-based reconstruction [19–22]. Several comparative studies between 2D and 3D GPR evaluations were performed with various gamma criteria, detector types, and 3D reconstruction types [47–50]. Kim et al. performed 2D gamma evaluations with EBT2 film and 3D gamma evaluations with the COMPASS™ system for 20 IMRT and VMAT plans, and no strong correlation was found between them [47]. Pulliam et al. performed 2D and 3D gamma analyses on 50 IMRT plans calculated with collapsed-cone convolution (CCC) and Monte Carlo (MC) simulations, and found higher GPRs in 3D than those in 2D up to 2.9% [48].

Another study with 11 prostate IMRT plans demonstrated that the 3D GPR evaluation was more sensitive to catching errors than the 2D-based approach, and a strong correlation was interestingly observed between 2D and 3D GPRs [50]. In another study with the OCTAVIOUS 4D system and a relatively large amount of plans (150 VMAT plans), no assured correlation was found between the 2D and 3D GPR evaluations [51]. Although reconstruction-based 3D GPR evaluation provides dose-volume histograms (DVHs) for both planned and actual delivery, a significant discrepancy between 3D reconstruction and 3D PAGAT gel dosimetry was reported [23]. Three-dimensional dosimeters are also known to inherently possess instability during manufacturing and calibration procedures, and difficulties in storage and reuse. Thus, 3D GPR evaluation is still insufficient as a standard for patient-specific QA [20,23,50].

In the multivariate regression results, the parameter combinations for each group agreed well with those of previous studies. For standard VMAT with Millennium MLC (group A), the best correlation was found with MU and MA combinations, although other combinations such as MU-$MI_s$ and $MI_s$-MA showed significant correlations. For standard VMAT with high-definition MLC where the jaw tracking mode was

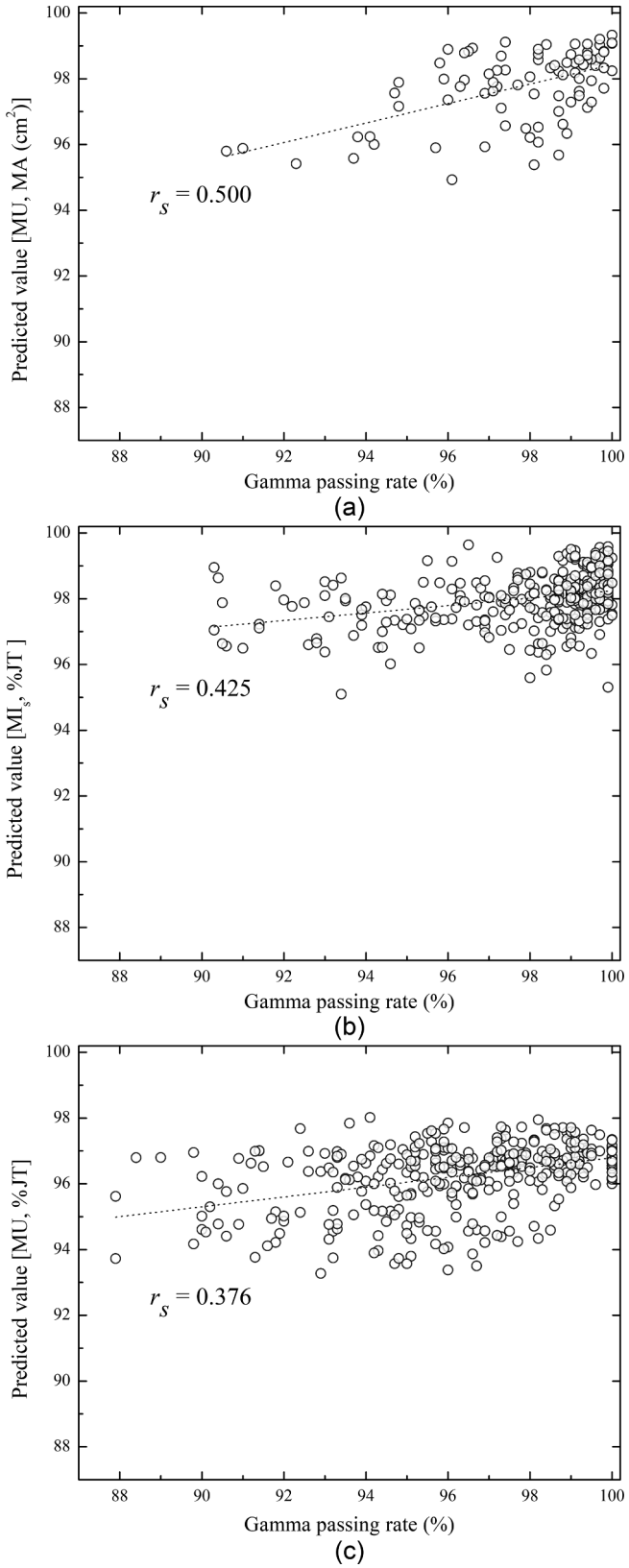


**Fig. 5.** Scatter plots of GPR and predicted value acquired by multiple parameter regression. Only one predicted value is presented as showing highest $r_s$ for GPR. (a) MU-MA combination for group A, (b) $MI_s$-%JT combination for group B, and (c) MU-%JT combination for group C.

available (group B), $MI_s$-%JT showed the highest $r_s$ with the GPR, while the single-parameter analysis gave $MI_s$ the highest correlation with GPR. Based on these results, the MLC modulation still remained the key parameter in the plan deliverability of group B. For stereotactic VMATs with high-definition MLC and jaw tracking availability (group C), the main factors were the total MU and the ratio of the jaw tracking rather than the MLC modulation. This suggests that a high positional accuracy of the collimators during MLC modulation with higher MU is the most critical parameter determining the high dosimetric accuracy in stereotactic VMAT delivery. For each treatment technique, specific plan parameters impacted individually or entirely on the plan deliverability [52,53].

As mentioned above, the strategies to minimize dosimetric uncertainties in small apertures, and trials combining 3D-based approaches, remain as future works. In addition, the establishment of detector and plan type-specific gamma criteria can provide more reliable systems to catch errors in patient-specific QA [14]. Moreover, further GPR evaluation in terms of aperture irregularities, edge area metrics, and circumference/area metrics will be performed in future investigations [39]. In our study, a single gamma criterion was applied to each group, leading to a relatively low discrimination in the correlation analysis (2 mm/2% for standard VMAT and 1 mm/2% for stereotactic VMAT). Nonetheless, the study outcome with a large amount of data can provide that the most influential parameters in VMAT delivery are associated with MLC modulation in standard VMAT, while those in stereotactic VMAT are correlated well with the amount of MU, amount of jaw tracking, and mean aperture sizes.

## 5. Conclusions

Various modulation indices such as $MI_s$, $MI_a$, and $MI_t$, along with plan parameters of MA, %JT, and MU were acquired and compared with GPR for 758 standard and stereotactic VMAT plans. The MLC modulation had the greatest impact on the GPR in standard VMAT plans regardless of the jaw tracking availability. In the case of stereotactic VMAT, where higher MUs and smaller field sizes were utilized compared to conventional fractionated radiotherapy, there was a greater influence owing to MU and %JT than MLC modulation.

## Declaration of Competing Interest

None.

## Acknowledgements

This work was supported by Radiation Technology R&D program through the National Research Foundation of South Korea funded by the Ministry of Science and ICT (No. 2017M2A2A7A02020641 and No. 2017M2A2A7A02020643).

## Appendix A

Previously devised modulation indices by Park et al

| Modulation index | Mathematical derivation | Description |
|---|---|---|
| $MI_s$ | $\text{MLC speed}_i = \frac{\lvert MLC_i - MLC_{i+1}\rvert}{\text{Time}_i} z_{\text{MLC speed}}(f) = \left(\frac{1}{(N_{CP}-1)}\right) N(f;\ \text{MLC speed}_i \rangle f \sigma_{\text{MLC speed}})$<br>$\text{Individual MI}_s = \int_0^k z_{\text{MLC speed}}(f)\,df \text{MI}_s = \sum_{n=1}^{120} \text{individual MI}_{s,n}$ | $MLC_i$: position of MLC[a] for $i$th CP[b] $\text{Time}_i$: time between $i$-th CP and $(i+1)$-th CP $\sigma_{MLC\ speed}$: standard deviation for MLC $\text{speed}_i$ $N_{CP}$: total number of CPs for a given VMAT[c] plan $N(f;\ \text{MLC speed}_i \rangle f \sigma_{\text{MLC speed}})$: count of number of changes for which $\text{MLC speed}_i \rangle f \sigma_{\text{MLC speed}}$ $n$: $n$th MLC leaf of linac[d] $\sigma_{MLC\ \text{accel}}$: standard deviation for MLC acceleration $\alpha$: weighting factor for acceleration $(1/\text{Time}_i)$ $N(f;\ \text{MLC speed}_i \rangle f \sigma_{\text{MLC speed}}$ or $\text{MLC accel}_i \rangle \alpha f \sigma_{\text{MLC accel}})$: count of number of changes for which $\text{MLC speed}_i \rangle f \sigma_{\text{MLC speed}}$ or $\text{MLC accel}_i \rangle \alpha f \sigma_{\text{MLC accel}}$ $GA_i$: gantry acceleration between $(i+1)$-th CP and $(i+2)$-th CP $DRV_i$: dose rate variation acceleration between $(i+1)$-th CP and $(i+2)$-th CP $W_{GA,i+1}$: weighting factors of variations of GA at $(i+1)$-th CP $W_{\text{MU},i+1}$: weighting factors of variations of DRV at $(i+1)$-th CP $\beta$: constant determining range of $W_{GA,i+1}$ $(\beta = 2)$ $\gamma$: constant for speed of convergence to maximum value of $W_{GA,i+1}$ |
| $MI_a$ | $\text{MLC accel}_i = \frac{\lvert \text{MLC speed}_i - \text{MLC speed}_{i+1}\rvert}{\text{Time}_i}$<br>$z_{\text{MLC accel}}(f) = \left(\frac{1}{(N_{CP}-2)}\right) N(f;\ \text{MLC speed}_i \rangle f \sigma_{\text{MLC speed}}\ or\ \text{MLC accel}_i \rangle \alpha f \sigma_{\text{MLC accel}})$<br>$\text{Individual MI}_a = \int_0^k z_{\text{MLC accel}}(f)\,df \text{MI}_a = \sum_{n=1}^{120} \text{individual MI}_{a,n}$ | |
| $MI_t$ | $GA_i = \left\lvert \frac{\Delta\text{Gantry angle}_i}{\text{Time}_i} - \frac{\Delta\text{Gantry angle}_{i+1}}{\text{Time}_{i+1}} \right\rvert \text{DRV}_i = \lvert \text{DR}_i - \text{DR}_{i+1} \rvert W_{GA,i+1} = \frac{\beta}{\{1+(\beta-1)\exp(-GA_i/\gamma)\}}$<br>$W_{MU,i+1} = \frac{\beta}{\{1+(\beta-1)\exp(-\text{DRV}_i/\gamma)\}}$<br>$z_{\text{total}}(f) = \left(\frac{1}{(N_{CP}-2)}\right) \sum_{i=1}^{N_{CP}} N_i(f;\ \text{MLC speed}_i \rangle f \sigma_{\text{MLC speed}}\ or\ \text{MLC accel}_i \rangle \alpha f \sigma_{\text{MLC accel}}) \cdot W_{\text{GA},i+1} \cdot W_{\text{MU},i+1}$<br>$\text{Individual MI}_t = \int_0^k z_{\text{total}}(f)\,df \text{MI}_t = \sum_{n=1}^{120} \text{individual MI}_{t,n}$ | |

[a] MLC: multileaf collimator.
[b] CP: control point.
[c] VMAT: volumetric modulated arc therapy.
[d] linac: linear accelerator.

## References

[1] Park JM, Kim K, Choi CH, Chie EK, Ye SJ, Ha SW. RapidArc® vs intensity-modulated radiation therapy for hepatocellular carcinoma: a comparative planning study. Br J Radiol 2010;85:e323–9.
[2] Otto K. Volumetric modulated arc therapy: IMRT in a single gantry arc. Med Phys 2008;35:310–7.
[3] Zhang P, Happersett L, Hunt M, Jackson A, Zelefsky M, Mageras G. Volumetric modulated arc therapy: planning and evaluation for prostate cancer cases. Int J Radiat Oncol Biol Phys 2010;76:1456–62.
[4] Teoh M, Clark C, Wood K, Whitaker S, Nisbet A. Volumetric modulated arc therapy: a review of current literature and clinical use in practice. Br J Radiol 2011;84:967–96.
[5] Chang BK, Timmerman RD. Stereotactic body radiation therapy: a comprehensive review. Am J Clin Oncol 2007;30:637–44.
[6] Guckenberger M, Andratschke N, Alheit H, Holy R, Moustakis C, Nestle U, et al. Definition of stereotactic body radiotherapy. Strahlenther Onkol 2014;190:26–33.
[7] Giglioli FR, Clemente S, Esposito M, Fiandra C, Marino C, Russo S, et al. Frontiers in planning optimization for lung SBRT. Phys Med 2017;44:163–70.
[8] Giglioli FR, Strigari L, Ragona R, Borzì GR, Cagni E, Carbonini C, et al. Lung stereotactic ablative body radiotherapy: a large scale multi-institutional planning comparison for interpreting results of multi-institutional studies. Phys Med 2016;32:600–6.
[9] Esposito M, Maggi G, Marino C, Bottalico L, Cagni E, Carbonini C, et al. Multicentre treatment planning inter-comparison in a national context: the liver stereotactic ablative radiotherapy case. Phys Med 2016;32:277–83.
[10] Aznar MC, Warren S, Hoogeman M, Josipovic M. The impact of technology on the changing practice of lung SBRT. Phys Med 2018;47:129–38.
[11] Low DA, Harms WB, Mutic S, Purdy JA. A technique for the quantitative evaluation of dose distributions. Med Phys 1998;25:656–61.
[12] Sumida I, Yamaguchi H, Das IJ, Kizaki H, Aboshi K, Tsujii M, et al. Intensity-

modulated radiation therapy dose verification using fluence and portal imaging device. J Appl Clin Med Phys. 2016;17:259–71.
[13] Son J, Baek T, Lee B, Shin D, Park SY, Park J, et al. A comparison of the quality assurance of four dosimetric tools for intensity modulated radiation therapy. Radiol Oncol 2015;49:307–13.
[14] J-i Kim, Park S-Y, Kim HJ, Kim JH, Ye S-J, Park JM. The sensitivity of gamma-index method to the positioning errors of high-definition MLC in patient-specific VMAT QA for SBRT. Radiat Oncol 2014;9:167.
[15] Nicolini G, Vanetti E, Clivio A, Fogliata A, Korreman S, Bocanek J, et al. The GLAaS algorithm for portal dosimetry and quality assurance of RapidArc, an intensity modulated rotational therapy. Radiat Oncol 2008;3:24.
[16] Fogliata A, Clivio A, Fenoglietto P, Hrbacek J, Kloeck S, Lattuada P, et al. Quality assurance of RapidArc in clinical practice using portal dosimetry. Br J Radiol 2011;84:534–45.
[17] J-i Kim, Choi CH, Park S-Y, An H, Wu H-G, Gamma Park JM. Evaluation with portal dosimetry for volumetric modulated arc therapy and intensity-modulated radiation. Therapy Prog Med Phys 2017;28:61–6.
[18] Park S-Y, Park JM, Ye S-J. Quantitative data to show effects of geometric errors and dose gradients on dose difference for IMRT quality assurance measurements. J Radiat Prot 2011;36:183–9.
[19] Gorjiara T, Hill R, Kuncic Z, Adamovics J, Bosi S, Kim JH, et al. Investigation of radiological properties and water equivalency of PRESAGE® dosimeters. Med Phys 2011;38:2265–74.
[20] Miften M, Olch A, Mihailidis D, Moran J, Pawlicki T, Molineu A, et al. Tolerance limits and methodologies for IMRT measurement-based verification QA: recommendations of AAPM Task Group No. 218. Med Phys 2018;45:e53–83.
[21] Sakhalkar H, Sterling D, Adamovics J, Ibbott G, Oldham M. Investigation of the feasibility of relative 3D dosimetry in the Radiologic Physics Center Head and Neck IMRT phantom using Presage/optical-CT. Med Phys 2009;36:3371–7.
[22] Wuu CS, Xu Y. Three-dimensional dose verification for intensity modulated radiation therapy using optical CT based polymer gel dosimetry. Med Phys 2006;33:1412–9.
[23] Stevens S, Dvorak P, Spevacek V, Pilarova K, Bray-Parry M, Gesner J, et al. An assessment of a 3D EPID-based dosimetry system using conventional two-and three-dimensional detectors for VMAT. Phys Med 2018;45:25–34.
[24] Park JM, Park S-Y, Kim H, Kim JH, Carlson J, Ye S-J. Modulation indices for volumetric modulated arc therapy. Phys Med Biol 2014;59:7315–40.
[25] Masi L, Doro R, Favuzza V, Cipressi S, Livi L. Impact of plan parameters on the dosimetric accuracy of volumetric modulated arc therapy. Med Phys 2013;40:071718.
[26] Bresciani S, Miranti A, Di Dia A, Maggio A, Bracco C, Poli M, et al. A pre-treatment quality assurance survey on 384 patients treated with helical intensity-modulated radiotherapy. Radiother Oncol 2016;118:574–6.
[27] Kim J-i, Park JM, Park S-Y, Choi CH, Wu HG, Ye S-J. Assessment of potential jaw-tracking advantage using control point sequences of VMAT planning. J Appl Clin Med Phys 2014;15:160–8.
[28] Swinnen AC, Öllers MC, Roijen E, Nijsten SM, Verhaegen F. Influence of the jaw tracking technique on the dose calculation accuracy of small field VMAT plans. J Appl Clin Med Phys 2017;18:186–95.
[29] Thongsawad S, Khamfongkhruea C, Tannanonta C. Dosimetric effect of jaw tracking in volumetric-modulated arc therapy. J Med Phys 2018;43:52–7.
[30] McNiven AL, Sharpe MB, Purdie TG. A new metric for assessing IMRT modulation complexity and plan deliverability. Med Phys 2010;37:505–15.
[31] Pardo E, Novais JC, Molina López MY, Maqueda SR. On flattening filter-free portal dosimetry. J Appl Clin Med Phys 2016;17:132–45.
[32] Park JM, Park S-Y, Kim H. Modulation index for VMAT considering both mechanical and dose calculation uncertainties. Phys Med Biol 2015;60:7101–25.
[33] Alexopoulos E. Introduction to multivariate regression analysis. Hippokratia 2010;14:23–8.
[34] Simeonova AO, Fleckenstein K, Wertz H, Frauenfeld A, Boda-Heggemann J, Lohr F, et al. Are three doses of stereotactic ablative radiotherapy (SABR) more effective than 30 doses of conventional radiotherapy? Transl Lung Cancer Res 2012;1:45–53.
[35] Heilemann G, Poppe B, Laub W. On the sensitivity of common gamma-index evaluation methods to MLC misalignments in Rapidarc quality assurance. Med Phys 2013;40:031702.
[36] J-i Kim, Chun M, Wu H-G, Chie EK, Kim HJ, Kim JH, et al. analysis with a gamma criterion of 2%/1 mm for stereotactic ablative radiotherapy delivered with volumetric modulated arc therapy technique: a single institution experience. Oncotarget 2017;8:76076–84.
[37] Park S-Y, Kim IH, Ye S-J, Carlson J, Park JM. Texture analysis on the fluence map to evaluate the degree of modulation for volumetric modulated arc therapy. Med Phys 2014;41:111718.
[38] Du W, Cho SH, Zhang X, Hoffman KE, Kudchadker RJ. Quantification of beam complexity in intensity-modulated radiation therapy treatment plans. Med Phys 2014;41:021716.
[39] Götstedt J, Karlsson Hauer A, Bäck A. Development and evaluation of aperture-based complexity metrics using film and EPID measurements of static MLC openings. Med Phys 2015;42:3911–21.
[40] Wu H, Jiang F, Yue H, Hu Q, Zhang J, Liu Z, et al. A comparative study of identical VMAT plans with and without jaw tracking technique. J Appl Clin Med Phys 2016;17:133–41.
[41] Jin H, Jesseph FB, Ahmad S. A comparison study of volumetric modulated Arc therapy quality assurances using portal dosimetry and MapCHECK 2. Prog Med Phys 2014;25:65–71.
[42] Keeling VP, Ahmad S, Jin H. A comprehensive comparison study of three different planar IMRT QA techniques using MapCHECK 2. J Appl Clin Med Phys 2013;14:222–33.
[43] Li Q, Deng X, Chen L, Huang X, Huang S. The angular dependence of a 2-dimensional diode array and the feasibility of its application in verifying the composite dose distribution of intensity-modulated radiation therapy. Chin J Cancer 2010;29:617–20.
[44] Jursinic PA, Sharma R, Reuter J. MapCHECK used for rotational IMRT measurements: step-and-shoot, TomoTherapy. RapidArc Med Phys 2010;37:2837–46.
[45] Rinaldin G, Perna L, Agnello G, Pallazzi G, Cattaneo G, Fiorino C, et al. Quality assurance of rapid arc treatments: performances and pre-clinical verifications of a planar detector (MapCHECK2). Phys Med 2014;30:184–90.
[46] Chen F, Rao M, Ye J, Wu J, Wong T, Saini J, et al. Are 2D detector arrays sufficient for VMAT quality assurance? Int J Radiat Oncol Biol Phys 2010;78:S822.
[47] J-i Kim, Choi CH, Wu H-G, Kim JH, Kim K, Park JM. Correlation analysis between 2D and quasi-3D gamma evaluations for both intensity-modulated radiation therapy and volumetric modulated arc therapy. Oncotarget 2017;8:5449.
[48] Pulliam KB, Huang JY, Howell RM, Followill D, Bosca R, O'Daniel J, et al. Comparison of 2D and 3D gamma analyses. Med Phys 2014;41.
[49] Valve A, Keyriläinen J, Kulmala J. Compass model-based quality assurance for stereotactic VMAT treatment plans. Phys Med 2017;44:42–50.
[50] Zhang D, Wang B, Zhang G, Ma C, Deng X. Comparison of 3D and 2D gamma passing rate criteria for detection sensitivity to IMRT delivery errors. J Appl Clin Med Phys 2018;19:230–8.
[51] Rajasekaran D, Jeevanandam P, Sukumar P, Ranganathan A, Johnjothi S, Nagarajan V. A study on correlation between 2D and 3D gamma evaluation metrics in patient-specific quality assurance for VMAT. Med Dosim 2014;39:300–8.
[52] Mancosu P, Reggiori G, Alongi F, Cozzi L, Fogliata A, Lobefalo F, et al. Total monitor units influence on plan quality parameters in volumetric modulated arc therapy for breast case. Phys Med 2014;30:296–300.
[53] Russo S, Esposito M, Hernandez V, Saez J, Rossi F, Paoletti L, et al. Does deep inspiration breath hold reduce plan complexity? Multicentric experience of left breast cancer radiotherapy with volumetric modulated arc therapy. Phys Med 2019;59:79–85.